GEOPHYSICS, VOL. 74, NO. 6 (NOVEMBER-DECEMBER 2009); P. I43–I53, 6 FIGS.
10.1190/1.3239518

DOI:10.1190/1.3239518

3D vector gravity potential and line integrals for the gravity anomaly of a rectangular prism with 3D variable density contrast

Xiaobing Zhou[1]

ABSTRACT

Three-dimensional rectangular prisms are building blocks for calculating gravity anomalies from irregular 3D mass bodies with spatially variable density contrasts. A 3D vector gravity potential is defined for a 3D rectangular prism with density contrast varying in depth and horizontally. The vertical component of the gravity anomaly equals the flux of the 3D vector gravity potential through the enclosed surface of the prism. Thus, the 3D integral for the gravity anomaly is reduced to a 2D surface integral. In turn, a 2D vector gravity potential is defined. The vertical component of the gravity anomaly equals the net circulation of the 2D vector gravity potential along the enclosed contour bounding the surfaces of the prism. The 3D integral for the gravity anomaly is reduced to 1D line integrals. Further analytical or numerical solutions can then be obtained from the line integrals, depending on the forms of the density contrast functions. If an analytical solution cannot be obtained, the line-integral method is semianalytical, requiring numerical quadratures to be carried out at the final stages. Singularity and discontinuity exist in the algorithm and the method of exclusive infinitesimal sphere or circle is effective to remove them. Then the vector-potential line-integral method can calculate the gravity anomaly resulting from a rectangular prism with density contrast, varying simply in one direction and sophisticatedly in three directions. The advantage of the method is that the constraint to the form of the density contrast is greatly reduced and the numerical calculation for the gravity anomaly is fast.

INTRODUCTION

To calculate the gravity anomaly of an irregular 3D mass body with spatially variable density contrast, the mass body usually is approximated as a collection of vertical 3D rectangular prisms in juxtaposition. The gravity anomaly from the whole mass body is an algebraic sum of the contributions of all vertical prisms at appropriate depths and distances from the observation point. This procedure is widely used in gravity-anomaly forward modeling and inversion (Danes, 1960; Nagy, 1966; René, 1986; Rao et al., 1990; García-Abdeslem, 1992; Bear et al., 1995; Barbosa et al., 1999; Silva et al., 2000; Gallardo-Delgado et al., 2003; García-Abdeslem, 2005; Chakravarthi and Sundararajan, 2007) and terrain corrections (Danés, 1982; García-Abdeslem and Martín-Atienza, 2001). Thus, rectangular prisms are building blocks for calculating the gravity anomaly of irregular 3D mass bodies.

For a slim rectangular prism, Danes (1960) obtains an approximate analytical expression for the gravity anomaly when the density contrast is a logarithmic function of depth. For such a model, horizontal dimensions of the prism are constant and negligible compared to the distance from observation point. For a rectangular prism, a closed-form equation for the gravity anomaly is derived by Nagy (1966) and Banerjee and Gupta (1977) when the density contrast is a constant, by Rao et al. (1990) and Gallardo-Delgado et al. (2003) when the density contrast is a quadratic function of depth, and by García-Abdeslem (2005) when the density contrast varies with depth following a cubic polynomial law. For more complicated forms of the density contrast function, the numerical method might need to be used to calculate the gravity anomaly. Reducing a 3D calculation to a 1D calculation is efficient and thus important in complicated gravity forward and inverse modeling.

Historically, increase of density and decrease of porosity with depth is of primary interest because of the mechanical compaction arising from the overburden and diagenesis resulting in reduced porosity and vertically layered structure (Cordell, 1973; Murthy and Rao, 1979; Rao, 1986; Chai and Hinze, 1988; Litinsky, 1989; Guspí, 1990; Rao et al., 1990; García-Abdeslem, 1992; Rao et al., 1994; Pohánka, 1998; Hansen, 1999; Zhang, et al., 2001; Gallardo-Delgado et al., 2003; Holstein, 2003; García-Abdeslem, 2005; García-Abdeslem et al., 2005; Silva et al., 2006; Chakravarthi and Sundararajan, 2007; Chappell and Kusznir, 2008; Zhou, 2008, 2009). However, because of complicated geological and geochemical processes in

Manuscript received by the Editor 12 January 2009; revised manuscript received 2 June 2009; published online 25 November 2009.
[1]Montana Tech of the University of Montana, Department of Geophysical Engineering, Butte, Montana, U.S.A. E-mail: xzhou@mtech.edu.

the diagenesis of rocks, metamorphism, intrusives, extrusive volcanics, and facies changes, the density contrast of earth material can also depend arbitrarily on horizontal positions (Martín-Atienza and García-Abdeslem, 1999; Zhang et al., 2001; Zhou, 2009). For instance, as a sediment ages, organic matter combines with mineral constituents largely by physical forces. Changes in the density distribution of sediments can be caused by changes in oxidation or reduction by the surface charges that bind the components into a composite aggregate (Becking and Moore, 1959).

Specifically, mechanisms that cause variability in density contrast include dipping layered intrusions (Ruotoistenmäki, 1992), folded sedimentary formations, exhumation, overpressure, salt that can result in off-normal compaction curves in sediments, fan development (Cordell, 1979), nonuniform stratification, physical and chemical cementation (Vajk, 1956), and gradual horizontal change in density between two rock types caused by metamorphism (Gendzwill, 1970; Pan, 1989; Ruotoistenmäki, 1992). The density contrast of earth material also can depend arbitrarily on horizontal position (Martín-Atienza and García-Abdeslem, 1999; Zhang et al., 2001; Zhou, 2009).

Using line integrals is an efficient method to calculate the gravity anomaly for a given density-contrast model (Talwani et al., 1959; Zhou, 2008, 2009). Hubbert (1948) obtains a line integral for irregular 2D masses of constant density contrast for calculating the gravity anomaly. This is the basis for the classic Talwani et al. (1959) scheme for rapid computation. Murthy and Rao (1979) extend Hubbert's line integral to cases when the mass-density contrast is a function of depth. Zhou (2008, 2009) studies line integrals systematically for irregular 2D masses by defining a 2D vector gravity potential and obtains line integrals when the density contrast is depth-dependent or varies vertically and horizontally.

However, all of these line integrals are for 2D irregular mass bodies. My objective is to first define a 3D vector gravity potential and, subsequently, 2D vector gravity potentials for a 3D rectangular prism, with the density contrast dependent on depth or on depth and horizontal positions. Then, I reduce 3D integrals to 1D line integrals to calculate the gravity anomaly. Finally, I apply this vector-potential line-integral method to case studies to demonstrate its validity and capability when calculating the gravity anomaly from 3D prism mass bodies with simple to sophisticated forms of density contrast.

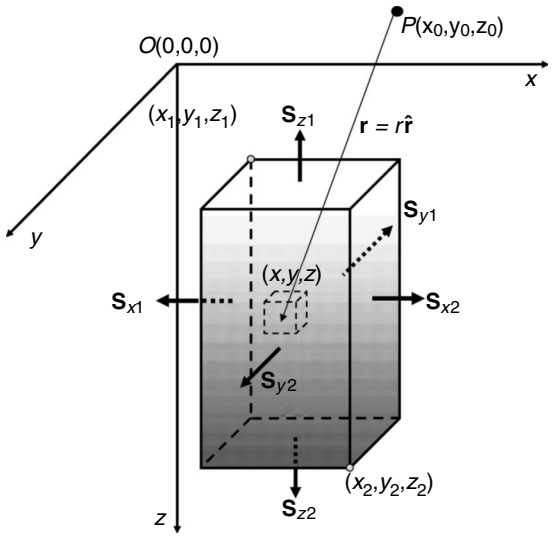

Figure 1. Drawing demonstrating the gravity anomaly at an observation point $P(x_0,y_0,z_0)$ resulting from a mass element at source point (x,y,z).

3D VECTOR GRAVITY POTENTIAL

Consider the geometry of the rectangular prism in Figure 1. The prism is bounded by six planar surfaces: S_{x1}, S_{x2}; S_{y1}, S_{y2}; and S_{z1}, S_{z2}. The direction of each surface normally points outward from the prism. Therefore, $\mathbf{S}_{x1} = -S_{x1}\hat{\mathbf{i}}$, $\mathbf{S}_{x2} = S_{x2}\hat{\mathbf{i}}$; $\mathbf{S}_{y1} = -S_{y1}\hat{\mathbf{j}}$, $\mathbf{S}_{y2} = S_{y2}\hat{\mathbf{j}}$; and $\mathbf{S}_{z1} = -S_{z1}\hat{\mathbf{k}}$, $\mathbf{S}_{z2} = S_{z2}\hat{\mathbf{k}}$, where $\hat{\mathbf{i}},\hat{\mathbf{j}},\hat{\mathbf{k}}$ are unit vectors along the x-, y-, and z-axes, respectively. An infinitesimal mass difference $dm = \Delta\rho dV$ between a 3D mass and its background is at point (x,y,z), where $\Delta\rho$ is the density contrast and $dV = dxdydz$ is the infinitesimal volume. The observation point is at point $P(x_0,y_0,z_0)$. From Newton's law, the magnitude of attraction on a unit mass at point P arising from the infinitesimal mass dm at distance r_0 is given by

$$d\mathbf{F} = G\frac{dm}{r_0^2}\hat{\mathbf{r}} = G\frac{\Delta\rho dV}{r_0^2}\hat{\mathbf{r}}, \tag{1}$$

where G is Newton's gravitational constant, r_0 is the distance between the observation point and the mass source $dm = \Delta\rho dV$, and $\hat{\mathbf{r}}$ is the unit vector in the direction from the observation point to the mass source. The displacement vector from the observation point to the mass source is $\mathbf{r} = r_0\hat{\mathbf{r}} = (x - x_0)\hat{\mathbf{i}} + (y - y_0)\hat{\mathbf{j}} + (z - z_0)\hat{\mathbf{k}}$. The vertical component of the gravity anomaly observed at point $P(x_0,y_0,z_0)$ is

$$\Delta g_z(x_0,y_0,z_0) = G\int_V \frac{\Delta\rho dV}{r_0^2}\hat{\mathbf{k}}\cdot\hat{\mathbf{r}} = G\int_V \frac{(z - z_0)\Delta\rho}{r_0(x,y,z)^3}dydxdz, \tag{2}$$

with

$$r_0(x,y,z) = \sqrt{(x - x_0)^2 + (y - y_0)^2 + (z - z_0)^2}.$$

The divergence theorem shows that for vector $\mathbf{A}$, the volume integral of $\nabla\cdot\mathbf{A}$ equals the total outward flux of it through the closed surface bounding the volume:

$$\int_V \nabla\cdot\mathbf{A}dV = \oint_S \mathbf{A}\cdot d\mathbf{s}, \tag{3}$$

where $d\mathbf{s}$ is an infinitesimal surface area vector, with direction being normal to the surface but outward from the volume, and S is the closed surface bounding the volume. Comparing equation 3 with equation 2, to convert the volume integral for the gravity anomaly to a surface integral (SI), we need only find a vector $\mathbf{A}$ satisfying

$$\nabla\cdot\mathbf{A} = \frac{\partial A_x}{\partial x} + \frac{\partial A_y}{\partial y} + \frac{\partial A_z}{\partial z} = \frac{G(z - z_0)\Delta\rho}{r_0(x,y,z)^3}. \tag{4}$$

Thus, the vertical component of the gravity anomaly caused by a 3D mass body takes the form

$$\Delta g_z(x_0,y_0,z_0) = \oint_S \mathbf{A}\cdot d\mathbf{s}. \tag{5}$$

Similar to defining a 2D vector gravity potential (Zhou, 2008), we define the vector potential $\mathbf{A}$ that satisfies equation 4 as a 3D vector

gravity potential so that the gravity anomaly caused by a 3D mass equals the total flux of the 3D vector potential through the closed surface bounding the mass.

Because the divergence of the curl of any vector field is identically zero, i.e., for any vector field $\mathbf{E}(x,y,z)$, $\nabla\cdot(\nabla\times\mathbf{E})=0$, we have

$$\nabla\cdot\mathbf{A}=\nabla\cdot(\mathbf{A}+\nabla\times\mathbf{E}), \tag{6}$$

which means the 3D vector gravity potential defined by equation 4 is not unique, but the gravity anomaly calculated by various 3D vector gravity potentials satisfying equation 4 should be exactly the same, as determined by equation 5. This nonuniqueness of the 3D vector gravity potential combined with the uniqueness of the gravity anomaly provides many options for gravity-anomaly calculation using equation 5 by selecting different 3D vector gravity potentials ($\mathbf{A}$) for different forms of the density-contrast function.

Based on the selected 3D vector gravity potential, the 2D surface integral can be further converted into line integrals (Zhou, 2008, 2009). Therefore, the gravity-anomaly calculation of a 3D mass body eventually can be converted into a line-integral calculation. Compared with the 3D vector gravity potential method here, the calculation can be simplified greatly by appropriate selection of the 3D vector gravity potential. This point is elucidated in the following discussion.

LINE INTEGRALS FOR A RECTANGULAR PRISM WITH DEPTH-DEPENDENT DENSITY CONTRAST

For the rectangular prism shown in Figure 1, when the density contrast depends only on the depth z, i.e., $\Delta\rho=\Delta\rho(z)$, we select the 3D vector gravity potential satisfying equation 4 as

$$\begin{cases} A_y=A_z=0, \\ A_x=\dfrac{G(z-z_0)(x-x_0)\Delta\rho(z)}{r_0(x,y,z)[(y-y_0)^2+(z-z_0)^2]}. \end{cases} \tag{7}$$

It is easy to see that equation 7 satisfies equation 4. Inserting the above 3D vector potential (equation 7) in equation 5, the total flux of the 3D vector gravity potential through the closed surface of the 3D mass body becomes

$$\Delta g_z(x_0,y_0,z_0)=-\int\int_{S_{x1}}A_{x1}dydz+\int\int_{S_{x2}}A_{x2}dydz. \tag{8}$$

Setting $i=1$ or 2, then A_{x1} and A_{x2} in equation 8 satisfy

$$A_{xi}=\frac{G(z-z_0)(x_i-x_0)\Delta\rho(z)}{r_0(x,y,z)[(y-y_0)^2+(z-z_0)^2]}. \tag{9}$$

We convert the areal integrals in equation 8 to line integrals according to Stokes' theorem. Let's consider

$$I_i=\int\int_{S_{xi}}A_{xi}(y,z)dydz. \tag{10}$$

Surface S_{xi} is the vertical cross section of constant x (S_{x1} or S_{x2}), as shown in Figure 2a for the rectangular prism. We define the 2D vector gravity potential $\mathbf{B}_i$ satisfying

$$I_i=\int_S(\nabla\times\mathbf{B}_i)\cdot d\mathbf{s}=\int\int_S\left(\frac{\partial B_{iz}}{\partial y}-\frac{\partial B_{iy}}{\partial z}\right)dydz=-\oint_{C_1}(B_{iy}dy+B_{iz}dz), \tag{11}$$

where $d\mathbf{s}$ is an infinitesimal area element in $\mathbf{S}_{x2}$, the direction of which points to the x-axis ($\hat{\mathbf{i}}$), and C_1 is the contour of the parallelogram shown in Figure 2a. The line integral is counterclockwise along the contour, so the direction of $d\mathbf{s}$ and that of integration along the contour C_1 satisfy the right-hand rule.

The 2D vector gravity potential $\mathbf{B}_i$ that satisfies equation 10 is chosen as follows:

$$\begin{cases} B_{iy}=0, \\ B_{iz}=\displaystyle\int A_{xi}(y,z)dy=G(x_i-x_0)(z-z_0)\Delta\rho(z)I_{iz}, \end{cases} \tag{12}$$

where

$$I_{iz}=\int\frac{dy}{r_0(x,y,z)[(y-y_0)^2+(z-z_0)^2]}.$$

According to Banerjee and Gupta (1977), I_{iz} takes the following form:

$$I_{iz}=\frac{1}{(x_i-x_0)(z-z_0)}\tan^{-1}\left(\frac{(x_i-x_0)(y-y_0)}{(z-z_0)r_0(x,y,z)}\right). \tag{13}$$

Therefore, the vertical component of the gravity anomaly (equation 8) becomes

$$\Delta g_z(x_0,y_0,z_0)=-G\oint_{C_1}\Delta\rho(z)\times\left[\tan^{-1}\left(\frac{(x-x_0)(y-y_0)}{(z-z_0)r_0(x,y,z)}\right)\right]\Bigg|_{x_1}^{x_2}dz, \tag{14}$$

where $f(x)|_{x_1}^{x_2}=f(x_2)-f(x_1)$ is implied. Equation 14 is the line in-

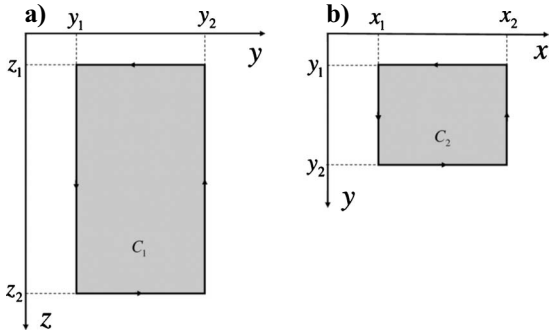

Figure 2. (a) Cross section of the rectangular prism projected onto a y-z-plane; C_1 is the closed contour bounding the cross section. (b) Cross section of the rectangular prism projected onto an x-y-plane; C_2 is the closed contour bounding the cross section.

tegral for the 3D rectangular prism with an arbitrarily depth-dependent density contrast. The gravity anomaly from a 3D rectangular prism becomes a line integral with an arctangent kernel.

Because the contour consists of four line segments (Figure 2a), $dz = 0$ for the top and bottom segments. Combining the integrals for all segments, we have

$$\Delta g_z(x_0,y_0,z_0) = G\int_{z_1}^{z_2}\Delta\rho(z) \times\left[\tan^{-1}\left(\frac{(x-x_0)(y-y_0)}{(z-z_0)r_0(x,y,z)}\right)\Bigg|_{x_1}^{x_2}\Bigg|_{y_1}^{y_2}\right]dz, \tag{15}$$

where $f(x,y)|_{x_1}^{x_2}|_{y_1}^{y_2} = f(x_2,y_2) + f(x_1,y_1) - f(x_2,y_1) - f(x_1,y_2)$ is implied. It reduces to the formula obtained by Garcia-Abdeslem (1992) when $x_0 = y_0 = z_0 = 0$. This derivation demonstrates that through appropriate selection of 3D and 2D vector gravity potentials, the volume integral for the gravity anomaly from a 3D mass can effectively be reduced to a line integral, making computation more efficient.

LINE INTEGRALS FOR A RECTANGULAR PRISM WITH HORIZONTALLY DEPENDENT DENSITY CONTRAST

Now consider that the density contrast depends horizontally on x and y, i.e., $\Delta\rho = \Delta\rho(x,y)$. It can be verified that

$$\frac{\partial}{\partial z}\left[\frac{G\Delta\rho(x,y)}{r_0(x,y,z)}\right] = -\frac{G(z-z_0)\Delta\rho(x,y)}{r_0(x,y,z)^3}.$$

Therefore, we can select the 3D vector potential that satisfies equation 4 as follows:

$$\begin{cases} A_x = A_y = 0, \\ A_z = -\dfrac{G\Delta\rho(x,y)}{r_0(x,y,z)}. \end{cases} \tag{16}$$

Inserting the 3D vector potential in equation 5, the total flux of the 3D vector gravity potential through the surface of the 3D mass body becomes

$$\Delta g_z(x_0,y_0,z_0) = -\int\int_{S_{z1}} A_{z1}dxdy + \int\int_{S_{z2}} A_{z2}dxdy = -\int\int_{S_z}\frac{G\Delta\rho(x,y)}{r_0(x,y,z)}\Bigg|_{z_1}^{z_2}dxdy, \tag{17}$$

where S_z is the horizontal cross section of the prism, as shown in Figure 2b. Now we convert the areal integrals in equation 17 to line integrals following Zhou (2008). Consider the following model for the horizontally dependent density contrast to accommodate a broad variety of geologic formations, similar to the density-contrast model in a 2D case (Zhou, 2009):

$$\Delta\rho(x,y) = \varepsilon(x) + \nu(y) + \sum_{\ell=1}^{N_x}\sum_{m=1}^{N_y}\sigma_\ell(x)\omega_m(y). \tag{18}$$

The first and second terms in this density-model equation describe components of the density contrast that depend only on the x- and y-directions, respectively. The third term describes a sum of cross terms of the density contrast that depends on both x and y positions. Index $\ell = 1,2,\ldots,N_x$ and $m = 1,2,\ldots,N_y$. The number of functions that depend only on x and y are N_x and N_y, respectively; $\varepsilon(x)$ and $\sigma_\ell(x)$ are any function of x, and $\nu(y)$ and $\omega_m(y)$ are any functions of y. The vertical component of the gravity anomaly caused by the 3D mass becomes (Zhou, 2008)

$$\Delta g_z(x_0,y_0,z_0) = -\oint_{C_2}(B_x dx + B_y dy), \tag{19}$$

with the 2D vector potential $\mathbf{B}$ satisfying

$$\frac{\partial B_y}{\partial x} - \frac{\partial B_x}{\partial y} = -\frac{G\Delta\rho(x,y)}{r_0(x,y,z)}\Bigg|_{z_1}^{z_2}. \tag{20}$$

Equation 19 means that the gravity anomaly caused by a 3D mass is eventually equal to the net circulation of $\mathbf{B}$, counterclockwise along the closed contour C_2 of the horizontal cross section of the 3D mass, as shown in Figure 2b.

Horizontal density-contrast functions — Line integrals with a logarithmic kernel

Let us now consider cases in which the horizontally dependent density-contrast model is only a function of x: $\Delta\rho = \varepsilon(x)$. From equation 20, the 2D vector gravity potential $\mathbf{B}_1$ satisfies

$$\frac{\partial B_{1y}}{\partial x} - \frac{\partial B_{1x}}{\partial y} = -\frac{G\varepsilon(x)}{r_0(x,y,z)}\Bigg|_{z_1}^{z_2}. \tag{21}$$

By the nonuniqueness of the vector gravity potential, $\mathbf{B}_1$ can be chosen as

$$\begin{cases} B_{1x} = G\varepsilon(x)\ln[(y-y_0) + r_0(x,y,z)]\big|_{z_1}^{z_2} \\ B_{1y} = 0. \end{cases} \tag{22}$$

Inserting equation 22 in equation 19, the vertical component of the gravity anomaly becomes

$$\Delta g_z(x_0,y_0,z_0) = -G\oint_{C_2}\varepsilon(x)\ln[(y-y_0) + r_0(x,y,z)]\big|_{z_1}^{z_2}dx. \tag{23}$$

Equation 23 is a line integral with a logarithmic kernel for density contrast varying with horizontal position because it contains a logarithmic function in its integrand that is independent of the density function. Equation 23 shows that the gravity anomaly from a 3D rectangular prism with $\Delta\rho = \varepsilon(x)$ becomes a line integral with a logarithmic kernel.

Because the contour for the line integral in equation 23 consists of four line segments (Figure 2b), $dx = 0$ for the two vertical segments. Considering that integration along the contour is clockwise and combining the integrals for the top and bottom segments, it yields

$$\Delta g_z(x_0,y_0,z_0) = -G\int_{x_1}^{x_2}\varepsilon(x)\ln[(y-y_0) + r_0(x,y,z)]\big|_{z_1}^{z_2}\big|_{y_1}^{y_2}dx. \tag{24}$$

Consider the cases in which the horizontally dependent density-contrast model is only a function y: $\Delta\rho = \nu(y)$. Similarly, the 2D vector gravity potential $\mathbf{B}_2$ is chosen as

$$\begin{cases} B_{2x} = 0, \\ B_{2y} = -G\nu(y)\ln[(x-x_0) + r_0(x,y,z)]\big|_{z_1}^{z_2}, \end{cases} \tag{25}$$

so that the vertical component of the gravity anomaly takes the following line integral form:

$$\Delta g_z(x_0,y_0,z_0) = G\oint_{C_2} \nu(y)\ln[(x-x_0) + r_0(x,y,z)]\big|_{z_1}^{z_2} dy, \tag{26}$$

where the contour along which the line integral is performed is the same as in equation 23. Considering the contour shown in Figure 2b and the integration direction, equation 24 eventually can be reduced to

$$\Delta g_z(x_0,y_0,z_0) = -G\int_{y_1}^{y_2} \nu(y)\ln\left[(x-x_0) + r_0(x,y,z)\right]\big|_{z_1}^{z_2}\big|_{x_1}^{x_2} dy. \tag{27}$$

Equations 23 and 26 form the line-integral set for the gravity-anomaly calculation for a 3D rectangular prism with density contrast depending only on x and y, respectively.

Model for the horizontally dependent density contrast

Now consider the horizontal density model (equation 18). For the first two terms, the corresponding 2D vector gravity potentials $\mathbf{B}_1$ and $\mathbf{B}_2$ and the line integrals have been obtained as above. The 2D vector gravity potential and the line integrals for the third term need to be found. We define the integrals for $\sigma_\ell(x)$ and $\omega_m(y)$ as

$$\Sigma_\ell(x,y,z) = \int \frac{\sigma_\ell(x)}{r_0(x,y,z)} dx \tag{28}$$

and

$$\Omega_m(x,y,z) = \int \frac{\omega_m(y)}{r_0(x,y,z)} dy. \tag{29}$$

If the 2D vector gravity potential corresponding to the cross term $\sigma_\ell(x)\omega_m(y)$ is denoted as $\mathbf{B}_{3lm}$ from equation 20, it should satisfy

$$\frac{\partial B_{3\ell m,y}}{\partial x} - \frac{\partial B_{3\ell m,x}}{\partial y} = -G\left.\frac{\sigma_\ell(x)\omega_m(y)}{r_0(x,y,z)}\right|_{z_1}^{z_2}. \tag{30}$$

If the integration in equation 28 is easier to perform than in equation 29, $\mathbf{B}_{3\ell m}$ is chosen as

$$\begin{cases} B_{3\ell m,x} = 0, \\ B_{3\ell m,y} = -G\,\Sigma_l(x,y,z)\big|_{z_1}^{z_2}\omega_m(y). \end{cases} \tag{31}$$

Otherwise, $\mathbf{B}_{3\ell m}$ is chosen as

$$\begin{cases} B_{3\ell m,x} = G\sigma_\ell(x)\,\Omega_m(x,y,z)\big|_{z_1}^{z_2}, \\ B_{3\ell m,y} = 0. \end{cases} \tag{32}$$

By the superposition principle, for the horizontal density-contrast model (equation 18), the 2D vector gravity potential is $\mathbf{B} = \mathbf{B}_1 + \mathbf{B}_2 + \sum_{\ell=1}^{N_x}\sum_{m=1}^{N_y}\mathbf{B}_{3\ell m}$. If $\Sigma_\ell(x,y,z)\big|_{z_1}^{z_2}$ is easier to obtain than $\Omega_m(x,y,z)\big|_{z_1}^{z_2}$, then

$$\begin{cases} B_x = G\varepsilon(x)\ln[(y-y_0) + r_0(x,y,z)]\big|_{z_1}^{z_2}, \\ B_y = -G\nu(y)\ln[(x-x_0) + r_0(x,y,z)]\big|_{z_1}^{z_2} - G\sum_{\ell=1}^{N_x}\sum_{m=1}^{N_y}\Sigma_\ell(x,y,z)\big|_{z_1}^{z_2}\omega_m(y). \end{cases} \tag{33}$$

Inserting equation 33 in equation 19, the vertical component of the gravity anomaly becomes

$$\begin{aligned} \Delta g_z(x_0,y_0,z_0) = &-G\oint_{C_2} \varepsilon(x)\ln[(y-y_0) + r_0(x,y,z)]\big|_{z_1}^{z_2} dx \\ &+ G\oint_{C_2} \left\{ \nu(y)\ln[(x-x_0) + r_0(x,y,z)] \right. \\ &\left. + \sum_{\ell=1}^{N_x}\sum_{m=1}^{N_y}\Sigma_l(x,y,z)\omega_m(y) \right\}\Big|_{z_1}^{z_2} dy. \end{aligned} \tag{34}$$

If $\Omega_m(x,y,z)\big|_{z_1}^{z_2}$ is easier to obtain than $\Sigma_\ell(x,y,z)\big|_{z_1}^{z_2}$, the counterparts of equations 33 and 34 are, respectively,

$$\begin{cases} B_x = G\varepsilon(x)\ln[(y-y_0) + r_0(x,y,z)]\big|_{z_1}^{z_2} + G\sum_{\ell=1}^{N_x}\sum_{m=1}^{N_y}\sigma_l(x)\,\Omega_m(x,y,z)\big|_{z_1}^{z_2}, \\ B_y = -G\nu(y)\ln[(x-x_0) + r_0(x,y,z)]\big|_{z_1}^{z_2} \end{cases} \tag{35}$$

and

$$\begin{aligned} \Delta g_z(x_0,y_0,z_0) = &-G\oint_{C_2} \left\{ \varepsilon(x)\ln[(y-y_0) + r_0(x,y,z)] \right. \\ &\left. + \sum_{\ell=1}^{N_x}\sum_{m=1}^{N_y}\sigma_\ell(x)\Omega_m(x,y,z) \right\}\Big|_{z_1}^{z_2} dx \\ &+ G\oint_{C_2} \nu(y)\ln[(x-x_0) + r_0(x,y,z)]\big|_{z_1}^{z_2} dy. \end{aligned} \tag{36}$$

Equations 34 and 36 are called line integrals for the horizontal density-contrast model (equation 18). Further analytical (closed-form) solution or numerical calculation of the gravity anomaly is based on the line integrals, depending on the exact form of the density-contrast function. A 3D rectangular prism with a horizontally varying density contrast also can be converted to a line integral.

LINE INTEGRALS FOR A RECTANGULAR PRISM WITH DENSITY CONTRAST VARYING IN HORIZONTAL AND VERTICAL DIRECTIONS

If the density contrast of the rectangular prism varies vertically and horizontally in a way that can be expressed more generally as

$$\Delta\rho(x,y,z) = \beta(z) + \varepsilon(x) + \nu(y) + \sum_{\ell=1}^{N_x}\sum_{m=1}^{N_y}\sigma_\ell(x)\omega_m(y), \tag{37}$$

then the line integral for the gravity anomaly is the sum of equation 14 and either equation 34 or equation 36 by the superposition principle. Thus, the vertical component of the gravity anomaly from a prism with a variable density contrast satisfying equation 37 can be calculated by a line integral as

$$\begin{aligned}\Delta g_z(x_0,y_0,z_0) = &-G\oint_{C_2}\varepsilon(x)\ln[(y-y_0)+r_0(x,y,z)]\Big|_{z_1}^{z_2}dx\\ &+G\oint_{C_2}\left\{\nu(y)\ln[(x-x_0)+r_0(x,y,z)]\right.\\ &\left.+\sum_{\ell=1}^{N_x}\sum_{m=1}^{N_y}\Sigma_l(x,y,z)\omega_m(y)\right\}\Bigg|_{z_1}^{z_2}dy\\ &-G\oint_{C_1}\beta(z)\\ &\times\left[\tan^{-1}\left(\frac{(x-x_0)(y-y_0)}{(z-z_0)r_0(x,y,z)}\right)\Bigg|_{x_1}^{x_2}\right]dz\end{aligned} \tag{38}$$

or

$$\begin{aligned}\Delta g_z(x_0,y_0,z_0) = &-G\oint_{C_2}\left\{\varepsilon(x)\ln[(y-y_0)+r_0(x,y,z)]\right.\\ &\left.+\sum_{\ell=1}^{N_x}\sum_{m=1}^{N_y}\sigma_\ell(x)\Omega_m(x,y,z)\right\}\Bigg|_{z_1}^{z_2}dx\\ &+G\oint_{C_2}\nu(y)\ln[(x-x_0)+r_0(x,y,z)]\Big|_{z_1}^{z_2}dy\\ &-G\oint_{C_1}\beta(z)\\ &\times\left[\tan^{-1}\left(\frac{(x-x_0)(y-y_0)}{(z-z_0)r_0(x,y,z)}\right)\Bigg|_{x_1}^{x_2}\right]dz.\end{aligned} \tag{39}$$

Considering contours C_1 and C_2 as shown in Figure 2, these two line integrals can be simplified to

$$\begin{aligned}\Delta g_z(x_0,y_0,z_0) = &-G\int_{x_1}^{x_2}\varepsilon(x)\ln[(y-y_0)+r_0(x,y,z)]\Big|_{z_1}^{z_2}\Big|_{y_1}^{y_2}dx\\ &-G\int_{y_1}^{y_2}\left\{\nu(y)\ln[(x-x_0)+r_0(x,y,z)]\right.\\ &\left.+\sum_{\ell=1}^{N_x}\sum_{m=1}^{N_y}\Sigma_l(x,y,z)\omega_m(y)\right\}\Bigg|_{z_1}^{z_2}\Bigg|_{x_1}^{x_2}dy\\ &+G\int_{z_1}^{z_2}\beta(z)\\ &\times\left[\tan^{-1}\left(\frac{(x-x_0)(y-y_0)}{(z-z_0)r_0(x,y,z)}\right)\Bigg|_{x_1}^{x_2}\Bigg|_{y_1}^{y_2}\right]dz,\end{aligned} \tag{40}$$

when $\Sigma_\ell(x,y,z)|_{z_1}^{z_2}$ is easier to obtain than $\Omega_m(x,y,z)|_{z_1}^{z_2}$ or

$$\begin{aligned}\Delta g_z(x_0,y_0,z_0) = &-G\int_{x_1}^{x_2}\left\{\varepsilon(x)\ln[(y-y_0)+r_0(x,y,z)]\right.\\ &\left.+\sum_{\ell=1}^{N_x}\sum_{m=1}^{N_y}\sigma_\ell(x)\Omega_m(x,y,z)\right\}\Bigg|_{z_1}^{z_2}\Bigg|_{y_1}^{y_2}dx\\ &-G\int_{y_1}^{y_2}\nu(y)\ln[(x-x_0)+r_0(x,y,z)]\Big|_{z_1}^{z_2}\Big|_{x_1}^{x_2}dy\\ &+G\int_{z_1}^{z_2}\beta(z)\\ &\times\left[\tan^{-1}\left(\frac{(x-x_0)(y-y_0)}{(z-z_0)r_0(x,y,z)}\right)\Bigg|_{x_1}^{x_2}\Bigg|_{y_1}^{y_2}\right]dz\end{aligned} \tag{41}$$

when $\Omega_m(x,y,z)|_{z_1}^{z_2}$ is easier to obtain. Equations 40 and 41 are line integrals useful for calculating the gravity anomaly when the density-contrast function satisfies equation 37.

SINGULARITIES AND DISCONTINUITY

Singularities exist in the logarithm and arctangent subfunctions in equations 40 and 41 when the observation point is placed on any of the edges of the rectangular prism. If the observation point is outside the prism or on any of the facets but not on any of the edges of the rectangular prism, singularities do not exist.

First, let us consider the logarithmic integrals over y in equation 40 or 41. Each integral can be expanded into four integrals. For one integral involving the top surface coordinates (x_1,y_1,z_1), the integral is

$$\int_{y_1}^{y_2} \nu(y)\ln[(x_1-x_0)+r_0(x_1,y,z_1)]dy$$

$$=\int_{y_1}^{y_2} \nu(y)\ln[(x_1-x_0)+\sqrt{(x_1-x_0)^2+(y-y_0)^2+(z_1-z_0)^2}]dy. \quad (42)$$

Singularity occurs in equation 42 when $(x_1-x_0)+r_0=0$. For $(x_1-x_0)+r_0=0$, we must have $x_1\le x_0$, $z_1=z_0$ and $y_0=y$, with y taking any value between y_1 and y_2, inclusive (see Figure 1). This means that singularity occurs when the observation point is on the edge ($x=x_1$, $z=z_1$) parallel to the y-axis and on the surface plane where $z_0=z_1$, $y_1\le y_0\le y_2$, and $x_0>x_1$.

Similar analyses for the other three integrals show that singularity occurs when the observation points are on the other three edges of the prism that are parallel to the y-axis and on the surface plane where $z_2=z_0$, $y_1\le y_0\le y_2$, and $x_1<x_0$. Therefore, the singularity occurs in the logarithmic integrals $\int_{y_1}^{y_2}\nu(y)\ln[(x-x_0)+r(x,y,z)]\big|_{z_1}^{z_2}\big|_{x_1}^{x_2}dy$ in equation 40 or 41 when the observation point is on any of the four edges of the prism parallel to the y-axis and on the top ($z_1=z_0$) and bottom ($z_2=z_0$) surface planes with $y_1\le y_0\le y_2$ and $x_1<x_0$ (Figure 1).

Similar analyses on the logarithmic integrals over x in equation 40 or 41 lead to the conclusion that singularity occurs in the logarithmic integrals $\int_{x_1}^{x_2}\varepsilon(x)\ln[(y-y_0)+r_0(x,y,z)]\big|_{z_1}^{z_2}\big|_{y_1}^{y_2}dx$ in equation 40 or 41 when the observation point is on any of the four edges of the prism that are parallel to the x-axis and on the top ($z_1=z_0$) and bottom ($z_2=z_0$) surface planes with $x_1\le x_0\le x_2$ and $y_1<y_0$ (Figure 1).

Now, consider the arctangent integral in equation 40 and 41. It still can be expanded into four integrals. Consider one integral involving the top surface coordinates (x_1,y_1,z_1). The integral is

$$\int_{z_1}^{z_2}\beta(z)\tan^{-1}\left(\frac{(x_1-x_0)(y_1-y_0)}{(z-z_0)\sqrt{(x_1-x_0)^2+(y-y_0)^2+(z-z_0)^2}}\right)dz. \quad (43)$$

Singularity occurs when the argument of the arctangent function becomes the indeterminate form $0/0$. For the arctangent argument in equation 43 to reach this indeterminate form, we must have $z_0=z$ with z taking any value between z_1 and z_2 inclusive (see Figure 1) and one of the following conditions: (1) $x_0=x_1$, (2) $y_0=y_1$, or (3) $x_0=x_1$, $y_0=y_1$. This means that singularity occurs when the observation point is on the edge ($x=x_1$, $y=y_1$) that is parallel to the z-axis, on the surface planes of $x=x_1$ and $y=y_1$ with $z_1\le z\le z_2$. Combining with similar analyses for the other three integrals, we can conclude that for the arctangent integral in equations 40 and 41, singularity occurs when the observation point is on any of the four edges of the prism that is parallel to the z-axis and on the surface planes $x=x_1$, $y=y_1$, $x=x_2$, and $y=y_2$ with $z_1\le z\le z_2$.

However, for the arctangent integral in equations 40 and 41, an additional point needs to be considered. In equations 40 and 41, the range of arctangent function is defined within $[-\pi/2,\pi/2]$. For observation points that are not on the edge ($x=x_1$, $y=y_1$) that is parallel to the z-axis but are between planes $z=z_1$ and $z=z_2$, when the line integration path passes through $z=z_0$, the integrand has a flip in sign, resulting in discontinuity. This can cause problems when the line integral is calculated using a numerical method such as Gaussian quadratures. However, the discontinuity can be removed by separating the integration into two parts from z_1 to $z_0-\varepsilon$ and from $z_0+\varepsilon$ to z_2, then taking the limit as $\varepsilon\to 0$. In a general way, the discontinuity in an arctangent integral can be removed by rewriting the integral as

$$\int_{z_1}^{z_2}\beta(z)\tan^{-1}\left(\frac{c}{z-z_0}\right)dz$$

$$=\lim_{\varepsilon\to 0}\int_{z_1}^{z_0-\varepsilon}\beta(z)\tan^{-1}\left(\frac{c}{z-z_0}\right)$$

$$+\lim_{\varepsilon\to 0}\int_{z_0+\varepsilon}^{z_2}\beta(z)\tan^{-1}\left(\frac{c}{z-z_0}\right).$$

In numerical computation, ε is a small positive number.

In potential theory, the distance between the computation point and the source point appears in the denominator of the 3D volume integral of potential. Thus, when the computation point overlaps with any point on the surface or inside the 3D source body, singularity occurs. Consider two infinitesimal masses. Even though they touch each other, the centers of the masses never overlap. Point mass is only a mathematical model; physically, mass without volume does not exist. Measurement of gravity is more the case. No matter how small a gravimeter is, gravity cannot be measured on the surface of the source or inside the mass body without drilling a hole.

Removal or avoidance of singularity in calculating potential fields is discussed by other researchers (e.g., Okabe, 1979; Pohanka, 1988; Tsoulis and Petrović, 2001; Holstein, 2002; 2003). Okabe (1979) proposes a method to avoid singularities in computing gravitational potential and gravity of homogeneous polyhedral bodies. To remove numerical singularities in the closed form of a gravity field of a homogeneous polyhedral body, Pohanka (1988) proposes to insert a small positive distance ε in the term that involves the singular point.

Tsoulis and Petrović (2001) show that the singularity in the gravity field of a homogeneous polyhedral body can be removed if one treats the singularities in the usual way of potential field theory, excluding a small sphere or circle around the singular point. Error in the numerical calculation is lumped into the integral around the small number or small sphere or circle. This technique is used not only in gravity potential but also in resistivity modeling (Lowry et al., 1989).

Holstein (2002, 2003) studies the gravimagnetic anomaly for uniform polyhedra and polyhedra of spatially linear media and shows that the singularity involves the product of a small quantity with limit zero and a large quantity with limit infinity but with a limiting product of zero. For such cases, there is no need for an ε exclusion zone, although numerical integration still should be carried out in split ranges (using a quadrature rule that avoids the end point) because the integrand derivative is singular. For linear media, all integrations can be carried out analytically (Holstein, 2003).

Because the singularity for line integrals of equations 40 and 41 occurs on the edges of the prism and on surface planes of the mass body, it can be removed by adding an exclusive infinitesimal sphere with a very small radius ε centering at each edge or at the singularity point to prevent the observation point from being located on the singularity. If the limit of the argument of the arctangent or logarithmic

function that is usually a multivariate function can be found when an indeterminate form occurs, then this exclusive infinitesimal sphere method can be avoided completely.

However, the limit of a multivariate function usually is not easy to find. The exclusive infinitesimal sphere method is convenient and practical for avoiding divergence in numerical computation. To see the sensitivity of the calculated gravity anomaly to radius ε of the exclusive infinitesimal sphere, I consider the same rectangular prism as in García-Abdeslem (2005): $x_1 = 10$ km, $x_2 = 20$ km; $y_1 = 10$ km, $y_2 = 20$ km; and $z_1 = 0$ km, $z_2 = 8$ km. I also use the same cubic-polynomial density-contrast function that fits to density data in Green Canyon, located offshore Louisiana, U.S.A., in the Gulf of Mexico (Li, 2001):

$$\Delta\rho(z) = -0.7477 + 2.03435\times10^{-4}z - 2.6764\times10^{-8}z^2 + 1.4247\times10^{-12}z^3, \quad (44)$$

where density contrast is in grams per cubic centimeter and z is in meters. Assume we want to calculate the gravity anomaly at point ($x_0 = 15$ km, $y_0 = 10$ km, $z_0 = 0$ km) at one of the edges of the prism using equation 40 or 41. To remove the singularity, calculation is performed for the gravity observation point ($x_0 = 15$ km, $y_0 = 10$ km, $z_0 = -\varepsilon$), where ε is the radius of the exclusive sphere. Figure 3 shows the difference between the calculated gravity anomaly at various ε and that which occurs when $\varepsilon = 10^{-20}$ m at observation point ($x_0 = 15$ km, $y_0 = 10$ km, $z_0 = -\varepsilon$). If we take $z_0 = -10^{-20}$ m to represent the top surface of the prism $z_0 = 0$ m, the curve in Figure 3 represents the singular error. If the radius of the exclusive sphere is smaller than 0.18 m, the error will not exceed 1 μGal. For the case $\varepsilon = 10^{-5}$ m, the error is about 5.86×10^{-8} mGal.

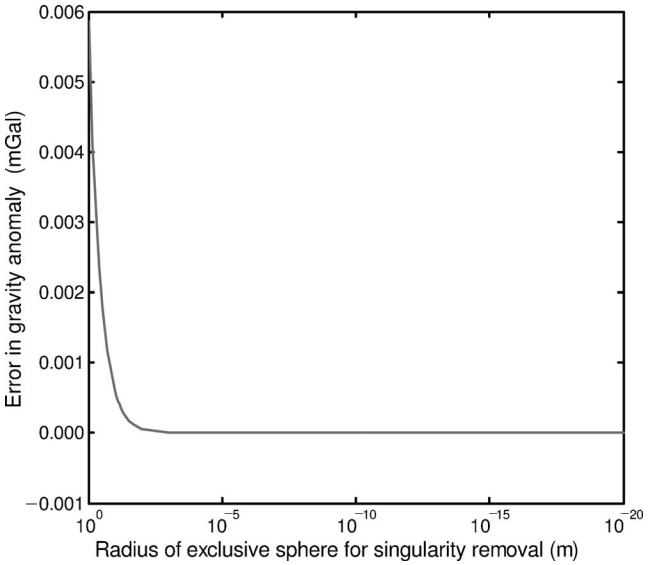

Figure 3. Difference between the gravity anomaly for various radius values of the exclusive infinitesimal sphere ε for singularity removal and that which occurs when $\varepsilon = 10^{-20}$ m at point ($x_0 = 15$ km, $y_0 = 10$ km, $z_0 = -\varepsilon$) for a prism determined by $x_1 = 10$ km, $x_2 = 20$ km; $y_1 = 10$ km, $y_2 = 20$ km; and $z_1 = 0$ km, $z_2 = 8$ km. The density contrast is given by equation 44. Taking the plane $\varepsilon = 10^{-20}$ m to represent the top surface of the prism, the difference represents the error arising from singularity removal when the gravity anomaly is supposed to be calculated at the point ($x_0 = 15$ km, $y_0 = 10$ km, $z_0 = 0$ km), which is on one edge of the prism.

One more point on singularity and discontinuity needs to be mentioned: If the observation point is inside the mass body, the rectangular prism can be cut into two, four, or eight subprisms so the observation point remains outside the prisms. Then, the gravity anomaly arising from the subprisms can be summed up. This is consistent with the reality that we cannot measure gravity inside the earth unless we drill a hole.

APPLICATION OF LINE INTEGRALS

The line integrals containing an arctangent kernel (third term) in equations 40 and 41 can be calculated quickly using the Gauss-Legendre quadrature method (Zhou, 2008). However, for the line integrals containing a logarithmic kernel (first and second terms) in equations 40 and 41. I found that using Romberg's method (Miller, 1970) is faster than the Gauss-Legendre quadrature method.

Case study: Density contrast varies with depth

This study is based on the same case as in Figure 3. To compare the results from the present line-integral method with those from the analytical solution derived by García-Abdeslem (2005), the gravity anomaly is calculated within the domain of $x_0 \in [0,30]$ km and $y_0 \in [0,30]$ km with equal intervals of $\Delta x_0 = \Delta y_0 = 0.5$ km at the same plane ($z_0 = -0.15$ m, corresponding to ε=0.15 m) to avoid singularity (García-Abdeslem, 2005). As discussed earlier, ε=0.15 m can result in an error of about 1 μGal. For a gravimeter with accuracy lower than 1 μGal, this choice is reasonable.

Figure 4a shows the gravity-anomaly distribution and contour lines of the gravity anomaly. Because the density contrast is symmetric about the $x = 15$ km and $y = 15$ km axes, the gravity anomaly should be symmetric about the same x- and y-axes. This salient feature is shown clearly in Figure 4a. Figure 4b illustrates the difference of the calculated gravity anomaly between the line-integral method and the analytical solution. The maximum difference is 1.0×10^{-6} mGal, which indicates that the line-integral method developed above agrees very well with the analytical solution.

Case study: Density contrast varying with depth and horizontal directions

To see the impact of the horizontal variation of density contrast on the gravity anomaly, let us consider a density transition zone where the horizontal variation of the density contrast can be approximated as horizontally linear (Gendzwill, 1970; Pan, 1989), although the dependence on depth takes the same form as equation 44. The density contrast for such a case is modeled as

$$\Delta\rho(z) = -0.7477 + 2.03435\times10^{-4}z - 2.6764\times10^{-8}z^2 + 1.4247\times10^{-12}z^3 - 2.32\times10^{-5}x, \quad (45)$$

where x is in meters. The gravity anomaly is calculated using equation 40 on the same surface domain for the same geometry of a prism as in Figure 4. Figure 5 shows the gravity anomaly distribution. Because the density contrast decreases with increasing x, the contour lines cluster toward the right edge of the prism. The density contrast is symmetrical about the $y = 15$ km axis, but no longer about the $x = 15{,}000$-m axis; so the gravity anomaly is expected to be symmetrical about the same y-axis, but no longer about the $x = 15{,}000$-m axis. This expected feature is shown clearly in Figure 5. The differ-

ence between Figures 5 and 4a is caused by the horizontal component in the density-contrast model: $\Delta\rho = -2.32\times10^{-5}x$.

To demonstrate the capability of the line integrals developed (equations 40 and 41) in calculating the gravity anomaly from a rectangular-prism mass body with a sophisticated dependence of the density contrast on space in all three directions, I consider a more complicated case:

$$\Delta\rho(x,y,z) = -0.623 + 4.37\times10^{-5}z + \frac{1.38}{12.6 + 2.3\times10^{-8}y^2} + (-0.28 + 3.6\times10^{-5}x) + (0.163 + 6.36\times10^{-5}x)\cos(3.2 + 9\times10^{-4}y), \quad (46)$$

where $\Delta\rho(x,y,z)$ is in g/cm^3, and x, y, and z are in meters. Comparing equation 46 with equation 37. I have $\varepsilon(x) = -0.28 + 3.6\times10^{-5}x$, $\nu(y) = 1.38/(12.6 + 2.3\times10^{-8}y^2)$, $\beta(z) = -0.623 + 4.37\times10^{-5}z$, $N_x = 1$, $N_y = 1$, $\omega_1(y) = \cos(3.2 + 9\times10^{-4}y)$, and $\sigma_1(x) = 0.163 + 6.36\times10^{-5}x$. Examining equations 28 and 29, $\Sigma_1(x,y,z)$ is easier to obtain than $\Omega_m(x,y,z)$. Inserting the expression for $\sigma_1(x)$ and $r_0(x,y,z) = \sqrt{(x-x_0)^2 + (y-y_0)^2 + (z-z_0)^2}$ in equation 28, we have

$$\Sigma_1(x,y,z) = \int \frac{0.163 + 6.36\times10^{-5}x}{\sqrt{(x-x_0)^2 + (y-y_0)^2 + (z-z_0)^2}}dx = (0.163 + 6.36\times10^{-5}x_0)\ln[x - x_0 + r_0(x,y,z)] + 6.36\times10^{-5}r_0(x,y,z).$$

Therefore, line-integral equation 40 is used to calculate the gravity anomaly.

Consider a rectangular prism with $(x_1,y_1,z_1) = (-5,-2,0)$ km, and $(x_2,y_2,z_2) = (5,2,10)$ km (see Figure 1). The gravity anomaly is calculated on the surface plane with the radius of exclusive infinitesimal sphere ε=0.01 m within the surface domain of $x_0 \in [-6$ km, $+6$ km] and $y_0 \in [-6$ km, $+6$ km] at an interval of 100 m in the x_0- and y_0-directions. Figure 6a shows the density-contrast distribution at the surface of the prism ($z = z_1 = 0$ km) and the contour lines. The density contrasts increase linearly with depth. The density distribution pattern in the x-y-plane at any depth is similar to Figure 6a. Surface distribution of the calculated gravity anomaly is shown in Figure 6b, where the contour lines at an interval of 4 mGal are also

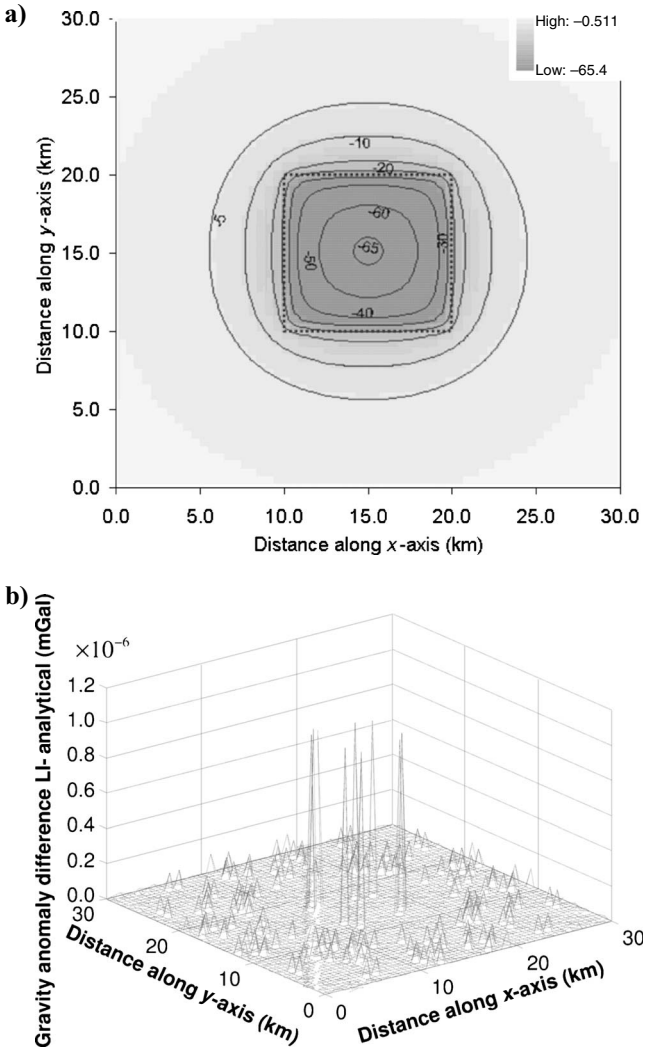

Figure 4. (a) Surface gravity-anomaly distribution using the line-integral method. The dotted line shows the edges of the top surface of the rectangular prism. Dimensions of the rectangular prism and the density function are discussed in the text. (b) Differences in the gravity anomalies calculated using the line integral method from those calculated using the analytical method (García-Abdeslem, 2005) are extremely small.

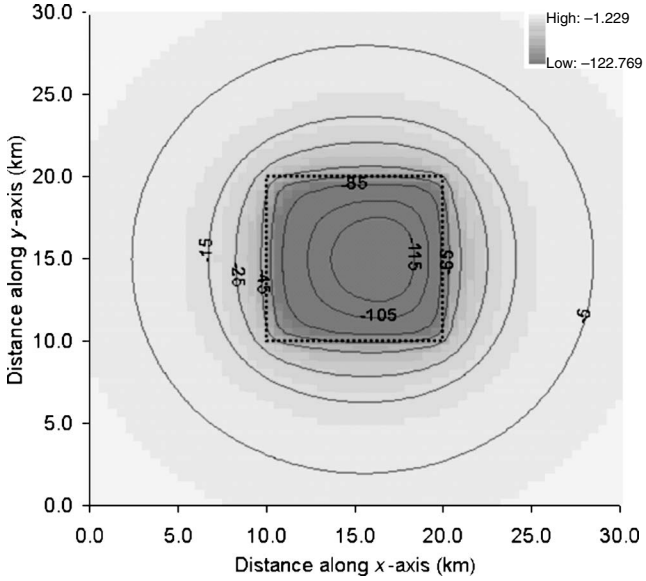

Figure 5. Surface gravity-anomaly distribution with contours of the gravity anomaly using the line-integral method. The dotted line shows the edges of the top surface of the rectangular prism. The density-contrast function is given by equation 45.

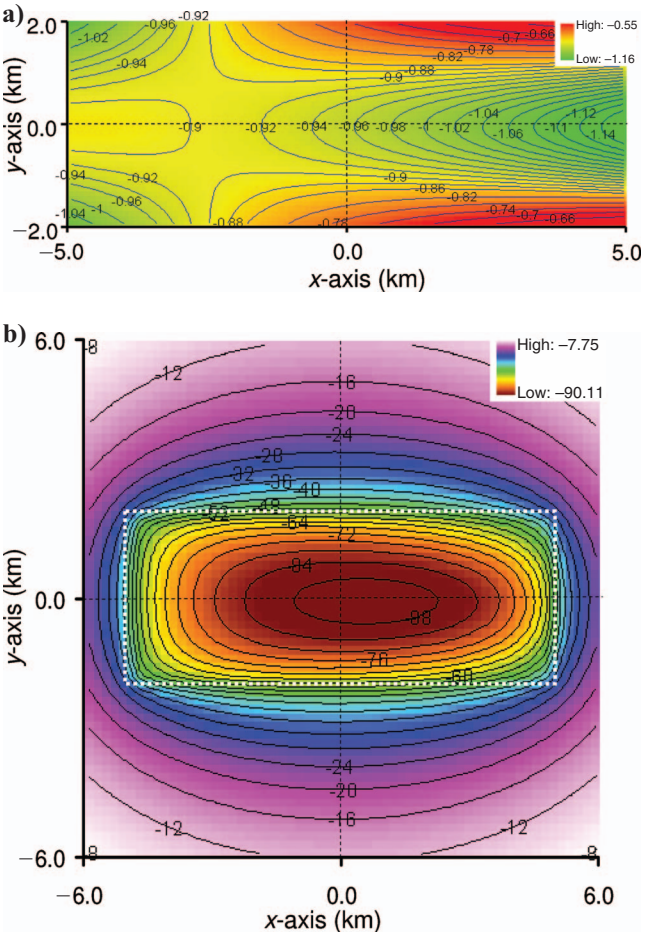

Figure 6. The dimensions of a rectangular prism are $(x_1,y_1,z_1) = (-5,-2,0)$ km and $(x_2,y_2,z_2) = (5,2,10)$ km. The density-contrast function is given by equation 46. (a) Horizontal distribution of the density contrast (in g/cm^3) at the top surface of a rectangular prism ($z = z_1 = 0$ km) and the contour lines. (b) Surface (x_0,y_0) distribution of the gravity anomaly at $z_0 = -0.01$ m plane. Contours of the gravity anomaly are shown with an interval of 4.0 mGal. The white dotted line shows the edges of the top surface of the prism.

depicted. Because the density contrast is asymmetric about the $x = 0$ and $y = 0$ planes, the gravity anomaly should be asymmetric about the x- and y-axes, as seen in Figure 6b.

CONCLUSIONS

This paper has focused on calculating the gravity anomaly of a 3D rectangular prism with a 3D variable density contrast because an irregular 3D mass body usually is approximated as a collection of vertical 3D rectangular prisms in juxtaposition. A 3D vector gravity potential is defined from the divergence theorem in vector calculus. As a consequence, the vertical component of the gravity anomaly of a 3D mass body is equal to the net flux of the 3D vector gravity potential through the closed surface bounding the mass.

The nonuniqueness of the 3D vector gravity potential and the uniqueness in the calculated gravity anomaly make it possible to select a form of the 3D vector gravity potential as simple as possible to convert the 3D volume integral to 2D areal integrals. In turn, the 2D areal integral was converted to 1D line integrals through defining a 2D vector gravity potential. Similarly, the nonuniqueness of the 2D vector gravity potential and the uniqueness in the calculated gravity anomaly made it possible to select a form of the 2D vector gravity potential as simple as possible to convert 2D areal integrals to 1D line integrals. Finally, a 3D volume integral for calculating the gravity anomaly was converted to 1D line integrals.

This procedure was performed for a sophisticated density-contrast model, depending on all three directions in the Cartesian coordinate system. Singularity occurs only when the observation point is located on the edges or surface planes of the prism, and removal was proposed by imposing an exclusive infinitesimal sphere with small radius ε concentric with the singularity point. To produce a gravity-anomaly calculation with accuracy greater than 1 μGal, $\varepsilon \le 0.1$ m was suggested; but the smaller the ε, the higher the accuracy. When a 3D volume integral was reduced to a 1D line integral, a volume with an order of N^3 internally discretized elementary grids was expected to have an order of N boundary elements. The number of integration steps can be reduced from an order of N^3 to an order of N. Savings of computation time is significant.

This vector-gravity-potential and line-integral method was applied to case studies to demonstrate its capability in calculating the gravity anomaly from a 3D rectangular prism with density contrast depending simply on one dimension to sophisticatedly on three directions.

ACKNOWLEDGMENTS

I am very grateful for the critique, helpful comments, and suggestions from reviewers Alex Chappell, Juan García-Abdeslem, Horst Holstein, and associate editor John W. Peirce.

REFERENCES

Banerjee, B., and S. P. D. Gupta, 1977, Gravitational attraction of a rectangular parallelepiped: Geophysics, **42**, 1053–1055.
Barbosa, V. C. F., J. B. C. Silva, and W. E. Medeiros, 1999, Gravity inversion of a discontinuous relief stabilized by weighted smoothness constraints on depth: Geophysics, **64**, 1429–1437.
Bear, G. W., H. J. Al-Shukri, and A. J. Rudman, 1995, Linear inversion of gravity data for 3-D density distributions: Geophysics, **60**, 1354–1364.
Becking, L. G. M. B., and D. Moore, 1959, Density distribution in sediments: Journal of Sedimentary Petrology, **29**, 47–55.
Chai, Y., and W. J. Hinze, 1988, Gravity inversion of an interface above which the density contrast varies exponentially with depth: Geophysics, **53**, 837–845.
Chakravarthi, V., and N. Sundararajan, 2007, 3D gravity inversion of basement relief — A depth-dependent density approach: Geophysics, **72**, no. 2., I23–I32.
Chappell, A., and N. Kusznir, 2008, An algorithm to calculate the gravity anomaly of sedimentary basins with exponential density-depth relationships: Geophysical Prospecting, **56**, 249–258.
Cordell, L., 1973, Gravity analysis using an exponential density-depth function — San Jacinto graben, California: Geophysics, **38**, 684–690.
———, 1979, Sedimentary facies and gravity anomaly across master faults of the Rio Grande rift in New Mexico: Geology, **7**, 201–205.
Danes, Z. F., 1960, On a successive approximation method for interpreting gravity anomalies: Geophysics, **25**, 1215–1228.
———, 1982, An analytic method for the determination of distant terrain corrections: Geophysics, **47**, 1453–1455.
Gallardo-Delgado, L. A., M. A. Pérez-Flores, and Enrique Gómez-Treviño, 2003, A versatile algorithm for joint 3D inversion of gravity and magnetic data: Geophysics, **68**, 949–959.
García-Abdeslem, J., 1992, Gravitational attraction of a rectangular prism with depth-dependent density: Geophysics, **57**, 470–473.
———, 2005, The gravitational attraction of a right rectangular prism with density varying with depth following a cubic polynomial: Geophysics, **70**, no. 6, J39–J42.
García-Abdeslem, J., and B. Martín-Atienza, 2001, A method to compute terrain corrections for gravimeter stations using a digital elevation model: Geophysics, **66**, 1110–1115.
García-Abdeslem, J., J. M. Romo, E. Gómez-Treviño, J. Ramírez-Hernán-

dez, F. J. Esparza-Hernández, and C. F. Flores-Luna, 2005, A constrained 2D gravity model of the Sebastián Vizcaíno basin, Baja California Sur, Mexico: Geophysical Prospecting, **53**, 755–765.
Gendzwill, D. J., 1970, The gradational density contrast as a gravity interpretation model: Geophysics, **35**, 270–278.
Guspí, F., 1990, General 2D gravity inversion with density contrast varying with depth: Geoexploration, **26**, 253–265.
Hansen, R. O., 1999, An analytical expression for the gravity field of a polyhedral body with linearly varying density: Geophysics, **64**, 75–77.
Holstein, H., 2002, Gravimagnetic similarity in anomaly formulas for uniform polyhedra: Geophysics, **67**, 1126–1133.
———, 2003, Gravimagnetic anomaly formulas for polyhedra of spatially linear media: Geophysics, **68**, 157–167.
Hubbert, M. K., 1948, A line-integral method of computing the gravimetric effects of two-dimensional masses: Geophysics, **13**, 215–225.
Li, X., 2001, Vertical resolution: Gravity versus vertical gravity gradient: The Leading Edge, **20**, 901–904.
Litinsky, V. A., 1989, Concept of effective density: Key to gravity depth determinations for sedimentary basins: Geophysics, **54**, 1474–1482.
Lowry, T., M. B. Allen, and P. N. Shive, 1989, Singularity removal: A refinement of resistivity modeling techniques: Geophysics, **54**, 766–774.
Martín-Atienza, B., and J. García-Abdeslem, 1999, 2-D gravity modeling with analytically defined geometry and quadratic polynomial density functions: Geophysics, **64**, 1730–1734.
Miller, E. K., 1970, A variable interval width quadrature technique based on Romberg's method: Journal of Computational Physics, **5**, 265–279.
Murthy, I. V. R., and D. B. Rao, 1979, Gravity anomalies of two-dimensional bodies of irregular cross-section with density contrast varying with depth: Geophysics, **44**, 1525–1530.
Nagy, D., 1966, The gravitational attraction of a right rectangular prism: Geophysics, **31**, 362–371.
Okabe, M., 1979, Analytical expressions for gravity anomalies due to homogeneous polyhedral bodies and translations into magnetic anomalies: Geophysics, **44**, 730–741.
Pan, J.-J., 1989, Gravity anomalies of irregularly shaped two-dimensional bodies with constant horizontal density gradient: Geophysics, **54**, 528–530.
Pohanka, V., 1988, Optimum expression for computation of the gravity field of a homogeneous polyhedral body: Geophysical Prospecting, **36**, 733–751.
———, 1998, Optimum expression for computation of the gravity field of a polyhedral body with linearly increasing density: Geophysical Prospecting, **46**, 391–404.
Rao, C. V., V. Chakravarthi, and M. L. Raju, 1994, Forward modelling: Gravity anomalies of two-dimensional bodies of arbitrary shape with hyperbolic and parabolic density functions: Computers and Geosciences, **20**, 873–880.
Rao, D. B., 1986, Modelling of sedimentary basins from gravity anomalies with variable density contrast: Geophysical Journal of the Royal Astronomical Society, **84**, 207–212.
Rao, D. B., M. J. Prakash, and N. Ramesh Babu, 1990, 3D and $2\frac{1}{2}$D modeling of gravity anomalies with variable density contrast: Geophysical Prospecting, **38**, 411–422.
René, R. M., 1986, Gravity inversion using open, reject, and "shape-of-anomaly" fill criteria: Geophysics, **51**, 988–994.
Ruotoistenmäki, T., 1992, The gravity anomaly of two-dimensional sources with continuous density distribution and bounded by continuous surfaces: Geophysics, **57**, 623–628.
Silva, J. B. C., D. C. L. Costa, and V. C. F. Barbosa, 2006, Gravity inversion of basement relief and estimation of density contrast variation with depth: Geophysics, **71**, no. 5, J51–J58.
Silva, J. B. C., W. E. Medeiros, and V. C. F. Barbosa, 2000, Gravity inversion using convexity constraint: Geophysics, **65**, 102–112.
Talwani, M., J. L. Worzel, and M. Landisman, 1959, Rapid gravity computations for two-dimensional bodies with application to the Mendocino submarine fracture zone: Journal of Geophysical Research, **64**, 49–59.
Tsoulis, D., and S. Petrović, 2001, On the singularities of the gravity field of a homogeneous polyhedral body: Geophysics, **66**, 535–539.
Vajk, R., 1956, Bouguer corrections with varying surface density: Geophysics, **21**, 1004–1020.
Zhang, J., B. Zhong, X. Zhou, and Y. Dai, 2001, Gravity anomalies of 2-D bodies with variable density contrast: Geophysics, **66**, 809–813.
Zhou, X., 2008, 2D vector gravity potential and line integrals for the gravity anomaly caused by a 2D mass of depth-dependent density contrast: Geophysics, **73**, no. 6, I43–I50.
———, 2009, General line integrals for gravity anomalies of irregular 2D masses with horizontally and vertically dependent density contrast: Geophysics, **74**, no. 2, I1–I7.